Wiley
International Journal of Energy Research
Volume 2025, Article ID 8352032, 13 pages
https://doi.org/10.1155/er/8352032

WILEY

Research Article

Agarose Hydrogel-Based Power Source: Electrode Potential Engineering and Flow System Integration for Enhanced and Sustained Performance

Sung-Hyun Kim,[1] Yang-Woo Lee,[1] Donghyeok Kim,[1] Jong-Bin Won,[2] Jeong Gon Son,[3,4] Jinhan Cho,[5] Ju-Hee So,[6,7] and Hyung-Jun Koo[1]

[1]*Department of Chemical and Biomolecular Engineering, Seoul National University of Science and Technology, Nowon-gu, Seoul 01818, Republic of Korea*
[2]*Department of Chemical Engineering, University of Michigan, Ann Arbor 48105, Michigan, USA*
[3]*Electronic and Hybrid Materials Research Center, Korea Institute of Science and Technology (KIST), Seongbuk-gu, Seoul 02792, Republic of Korea*
[4]*KU-KIST Graduate School of Converging Science and Technology, Korea University, Seongbuk-Gu, Seoul 02841, Republic of Korea*
[5]*Department of Chemical and Biological Engineering, Korea University, Seongbuk-gu, Seoul 02841, Republic of Korea*
[6]*User Convenience Technology R&D Department, Korea Institute of Industrial Technology, Ansan-Si 15588, Republic of Korea*
[7]*College of ICT Engineering, Chung-Ang University, Seoul 06974, Republic of Korea*

Correspondence should be addressed to Ju-Hee So; jso@kitech.re.kr and Hyung-Jun Koo; hjkoo@seoultech.ac.kr

Received 15 September 2025; Revised 21 November 2025; Accepted 3 December 2025

Academic Editor: Suresh Kannan Balasingam

Inspired by the electrical discharge mechanism of electric fish, we report a bio-inspired power source based on agarose hydrogels. The device generates electrical energy by exploiting ion concentration gradients across high- and low-salinity hydrogels, in combination with polyelectrolyte membrane gels exhibiting ion selectivity based on Donnan exclusion. Systematic optimization of hydrogel composition identified optimal ion concentrations and agarose content that balance energy output and mechanical stability. To further enhance performance, asymmetric redox pairs—ferrocyanide/ferricyanide at the anode and vanadium oxide at the cathode—were introduced, boosting both voltage and current outputs. Additionally, a continuous flow system was incorporated to replenish ionic gradients, addressing limitations from ion gradient depletion during extended operation. Simulations and experimental results confirmed that the flow-assisted configuration maintained stable ion distributions, enabling sustained power output over time. This work demonstrates a safe, scalable, and environmentally friendly platform for water-based energy harvesting, with potential applications in bio-interfacing and soft energy devices.

Keywords: agarose hydrogels; electric fish; flow systems; ion gradients; ion-selective membranes; redox pairs

1. Introduction

Among various strategies for bio-inspired energy conversion, electrochemical devices that mimic the electric energy generation mechanisms of electric fish, including species such as electric eels, catfish and rays, have been extensively investigated [1] due to their intrinsic modularity, compatibility with soft and aqueous systems, and potential for sustainable and biocompatible power generation. Electric fish generate electricity through the sequential activation of specialized cells called electrocytes, which act as biological capacitors by establishing transmembrane ion gradients and synchronously discharging them to produce high-voltage electric pulses. Electrocytes generate membrane potentials primarily by leveraging ion-selective membranes and sustaining transmembrane ion concentration gradients (Figure 1a). In the resting state without

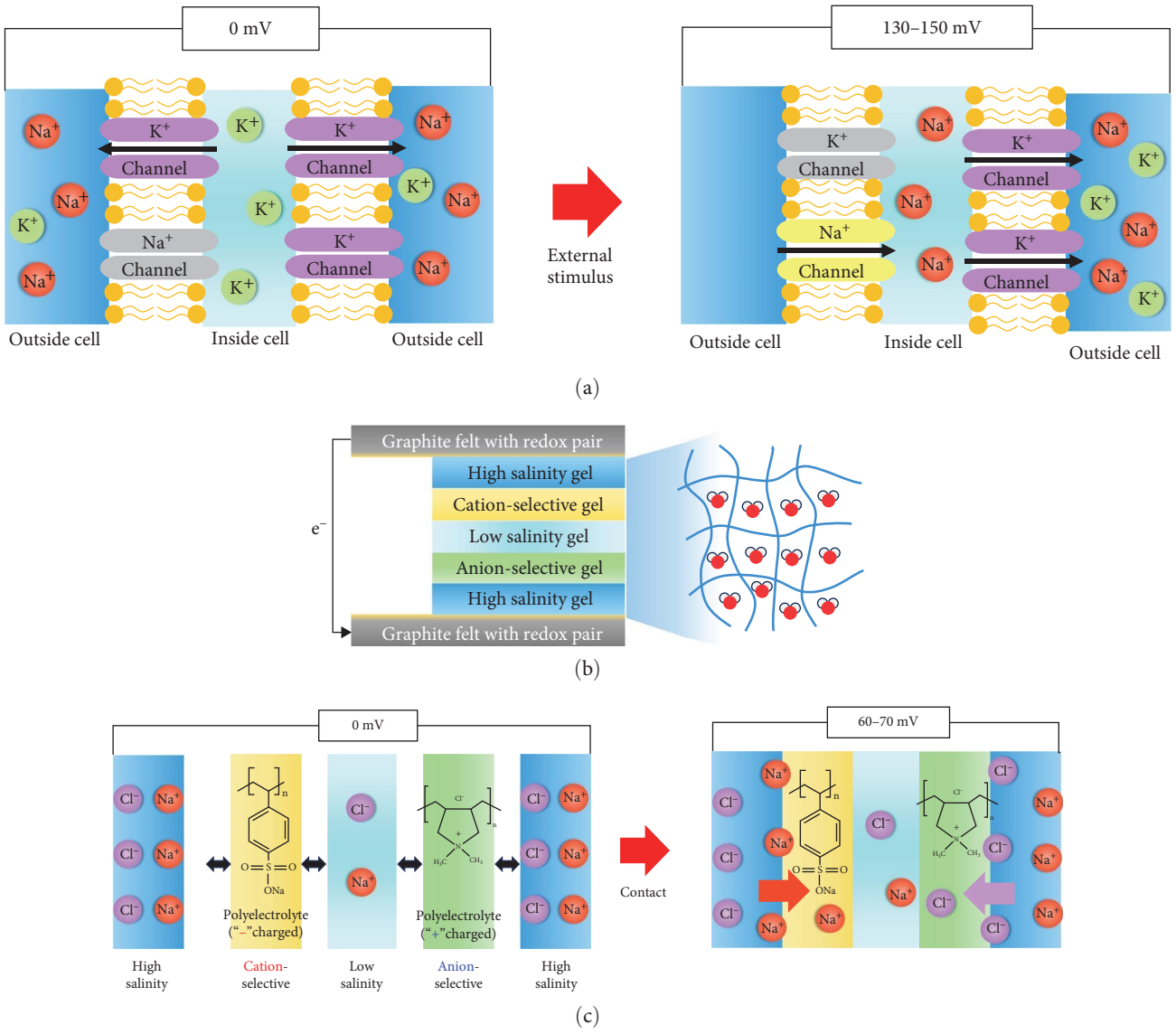

FIGURE 1: Schematic illustration of (a) the electric potential generation mechanism of electrocytes in the electric eel, (b) the structure of an agarose hydrogel-based power source, and (c) its power generation mechanism inspired by electrocytes.

external stimulation, a high concentration of Na^+ ions is maintained outside the electrocyte, while the intracellular space is rich in K^+ ions. The K^+ channels remain open, whereas the Na^+ channels are predominantly closed, maintaining the zero resting membrane potential. Upon receiving an external stimulus, neurons associated with the electrocyte are activated, triggering the opening of Na^+ channels and the closing of K^+ channels in the left membrane. Consequently, Na^+ ions flow into the cell from the extracellular space on the left side. Simultaneously, K^+ ions are transported from the intracellular to the extracellular region on the right side. This coordinated ion exchange results in an accumulation of positive charges outside the right side of the cell and a relative deficit of cations on the left side, thereby establishing a potential difference across the membrane. Through this process, each electrocyte can generate a potential difference of approximately 130–150 mV. The electrocytes of electric fish are organized in flattened plate-like structures that are arranged in series. The overall assembly of the electrocytes is reported to produce high voltages as high as 600 V [2, 3].

Hydrogels are frequently employed as matrix materials in energy devices designed to emulate the potential-generating mechanisms of electric fish [4–8]. The incorporation of hydrogels offers several advantages, as their high water content facilitates efficient ion transport while maintaining excellent biocompatibility. Additionally, hydrogels can be readily fabricated into diverse shapes and architectures through gelation processes [9–14]. Schroeder et al. [4] demonstrated a miniature system of artificial electrocyte cells based on polyacrylamide hydrogels fabricated via 3D printing and microfluidic assembly techniques, which enabled the mass production of cells subsequently connected in series. Each fabricated cell generated an open-circuit voltage in the range of approximately 130–185 mV, and by connecting thousands of such cells, a maximum output voltage of 110 V and a power density of approximately 27 mW/m^2 were achieved [4]. Guha et al. [7] reported a torpedo ray-inspired energy device

in which gel precursors were cast onto paper substrates and subsequently gelled, allowing the stacked paper layers to serve as the active elements. This approach resulted in thin-sheet devices capable of delivering a current density of upto 1.75 W/m^2 and a voltage of 250 mV per cell, with 16 stacked cells producing an overall output voltage of approximately 3.5 V [7]. In another example, Bütün et al. [8] fabricated similar bio-inspired energy devices based on poly(methyl methacrylate) blends with high ion conductivity. They investigated the effect of current collector metals on output voltage to maximize power generation. Most previous studies have relied on artificially synthesized polymers. In addition, the use of closed-system architectures leads to the gradual loss of ion concentration gradients due to ion diffusion, causing the output voltage and current to eventually decay to zero.

In this study, we developed an electric fish-inspired energy device utilizing ion concentration gradients within an agarose hydrogel matrix. Agarose, a natural polysaccharide extracted from red algae, is an economical, environmentally friendly, and highly biocompatible. It is capable of forming hydrogels with a water content exceeding 98%, and its mechanical strength can be readily adjusted by varying the polymer concentration [15–17]. Furthermore, agarose exhibits thermally reversible sol–gel transition behavior, which facilitates the fabrication of various geometries via general replica molding processes. Owing to these advantageous properties, agarose hydrogels have been widely applied as electrophoretic gel media [18, 19], scaffolds for cell culture and tissue engineering [20–22], and drug delivery systems [23, 24]. Their high ionic conductivity, derived from their substantial water content, has led to extensive research on integrating agarose hydrogels into diverse ionically driven devices [25]. In addition, physical incorporation of particles or polymers during gelation can impart new functionalities, such as ion selectivity [26, 27], photocatalytic activity [28–30], improved mechanical properties [31, 32], and enhanced ion conductivity [33, 34]. In this work, we incorporated a polyelectrolyte into the agarose hydrogel to immobilize charged species, thereby introducing ion selectivity.

To induce current generation in the bio-inspired devices with the established electrical potential, it was confirmed that the presence of redox pairs at both current collector interfaces was essential to promote charge transfer reactions and mitigate charge imbalance issues. Notably, as a novel strategy not previously explored, asymmetric redox pairs—ferricyanide/ferrocyanide and vanadium oxide—with different electrode potentials were introduced and experimentally evaluated for their ability to generate significantly enhanced output voltage and initial current. The effects of polyelectrolyte, agarose polymer, and ion concentrations on the output voltage and current were also investigated to optimize the hydrogel composition.

Finally, to enable long-term operation, we implemented a continuous flow system inspired by the design principles of a reverse electrodialysis (RED) power plant [35–38]. RED is a salinity-gradient energy harvesting technology that shares conceptual similarities with the electrochemical mechanism of electrocytes. In RED power plants, seawater and freshwater are continuously supplied through alternating ion-exchange membranes to generate electrical energy. Adopting this open, continuous-flow architecture to our soft hydrogel devices, we designed a low-flow channel system that continuously supply and drain saline solutions to maintain the ionic concentration gradient required for sustained operation. Numerical simulations were conducted to predict gradient sustainability, and the agreement between simulations and experiments demonstrates improved long-term stability.

2. Materials and Methods

2.1. Materials. Agarose (BioReagent, molecular biology, low EEO) for molecular biology, poly(sodium 4-styrenesulfonate) (PSS, 30 wt.% aqueous solution), poly(diallyldimethylammonium chloride) (PDAC, 20 wt.% aqueous solution), potassium hexacyanoferrate(II), potassium ferricyanide(III) (powder or chunks, <10 μm, 99%), potassium chloride (99%), and vanadium(IV) oxide sulfate hydrate (97%) were purchased from Sigma–Aldrich (NY, USA). Sodium chloride (99%) was purchased from DAE JUNG (Siheung, Republic of Korea). Graphite felt electrodes were supplied by Naracelltech Co., Ltd. (Seoul, Republic of Korea). Sulfuric acid (70%) was purchased from Samchun Chemicals (Seoul, Republic of Korea). Multiwalled carbon nanotubes (CNTs, 3 wt.% dispersed in water, diameter: 20–30 nm, length: 10–30 μm) were acquired from Nanostructured & Amorphous Materials (TX, USA). Polydimethylsiloxane (PDMS) Sylgard 184A was sourced from Sewang Hightech Co., Ltd. (Gimpo, Republic of Korea), while the Sylgard 184A silicone elastomer curing agent was obtained from Dow Corning (MI, USA). Deionized (DI) water with a resistivity of 18.2 MΩ cm was utilized in all procedures. Prior to use, all gel solutions were preheated in an oven to ensure homogeneity.

2.2. Preparation of Hydrogel Layers and Device Assembly. Four types of hydrogels were employed as the functional components of the device: high-salinity gel, low-salinity gel, cation-selective gel, and anion-selective gel. The high-salinity gel solution was composed of 4 M NaCl and 2 wt.% agarose in DI water. The low-salinity gel solution contained 20 mM NaCl and 2 wt.% agarose in DI water. The cation- and anion-selective gel solutions were prepared using 1 M PSS or 1 M PDAC, respectively, along with 3 wt.% agarose and DI water. All gel solutions were stirred at 550 rpm for 1 h. Subsequently, each solution was heated in a microwave oven for 30 s and then cast into PDMS molds (1 cm × 2 cm). Gelation was performed at ambient temperature for 20 min. The contact area between the gels was 1 cm × 2 cm. The thickness of the low-salinity gel was 1 mm, while the thickness of the other gels was 2 mm.

Graphite current collectors were heat-treated in a furnace at 400°C for 1 h to render the surface hydrophilic [39]. Following this treatment, the electrodes were immersed for 1 min in either 5 mL of a premixed solution containing 100 mM $K_4(Fe[CN]_6)$, 100 mM $K_3(Fe[CN]_6)$, and 1 M KCl, or 5 mL of a mixed solution containing 1.6 M vanadium(IV) oxide and 2.8 M H_2SO_4 [40, 41], which had been thoroughly mixed for 30 min prior to use. After immersion, the electrodes were dried in an oven at 60°C for 10 min. Finally, 4 mL of a 3 wt.% CNT aqueous dispersion was applied to the graphite felt, which was

subsequently dried in an oven at 60°C for 20 min to complete the electrode fabrication.

The five prepared hydrogels were assembled in a stacked arrangement for contact. Graphite felt current collectors were placed in contact with both high-salinity gels at each end. The resulting device was connected to a Keithley 2450 Sourcemeter (Tektronix, Beaverton, OR, USA). The open-circuit potential (V_{oc}) was measured with no applied current, while the short-circuit current (J_{sc}) was recorded under zero applied voltage.

2.3. Implementation of the Flow System. A syringe pump (NE-4000, NY, USA) equipped with 30 mL syringes was used to deliver the high- and low-salinity solutions, thereby maintaining the concentration gradient across the device. Tygon tubing (inner diameter: 0.4 mm; outer diameter: 1.08 mm, Saint-Gobain, Paris, France) was connected to each syringe and attached to the PDMS spacers, defining the source and drain channels. Additional tubing was connected at the outlets. The system consisted of two source channels supplying a high-salinity solution (6 M NaCl solution) and one drain channel carrying DI water. The source channels were positioned to contact one side of each high-salinity gel, whereas the drain channel was placed between the two low-salinity gels. The contact area between each salinity gel and the flow channels was set to one-quarter of the total gel area. Copper tape was applied as a current collector by contacting both sides of the high-salinity gels. The assembly was stacked in the following order from bottom to top: source channel, high-salinity gel, ion-selective gel, low-salinity gel, drain channel, low-salinity gel, ion-selective gel, high-salinity gel, and finally, another source channel. To prevent potential leaks, two glass plates were placed on both sides and secured with clamps. The syringe pump was operated at a flow rate of 10 mL h^{-1}.

2.4. Simulation. The ion concentration distribution was simulated using COMSOL Multiphysics software (Comsol AB, Stockholm, Sweden) with the Transport of Diluted Species module. The governing equation for species i is expressed as a mass balance:

$$\frac{\partial c_i}{\partial t} = \nabla \cdot (D_i \nabla c_i) + R_i \ , \qquad (1)$$

where c_i is the concentration of species i (mol m^{-3}), D_i is the diffusion coefficient of species i (m^2 s^{-1}), and R_i represents the reaction term accounting for local generation or consumption (mol $m^{-3}s^{-1}$). This diffusion equation was solved under time-dependent conditions to capture the evolution of the concentration profiles. It was assumed that the flow rates of the source and drain solutions were sufficiently high to maintain constant concentrations within the source and drain channels, therefore, convective effects were negligible. Accordingly, the concentrations of the high-concentration source and low-concentration drain solutions were set to 6 and 0 M, respectively. All surfaces other than the specified interface between gels were assigned no-flux boundary conditions to prevent mass transfer across those boundaries.

The dimensions of the simulation domains were defined as follows: the high-salinity gel measured 1 cm × 2 cm × 0.3 cm, the low-salinity gel (1 cm × 2 cm × 0.2 cm), the ion-selective, polyelectrolyte gel (1 cm × 2 cm × 0.2 cm), and the source and drain PDMS chambers (0.5 cm × 1 cm × 0.3 cm). The diffusion coefficient of salt ionsin all agarose hydrogel layers was assumed to be identical at 1.64×10^{-9} m^2s^{-1} [42]. The physical and chemical properties of the polyelectrolyte hydrogel were assumed to be identical to those of the pristine agarose gel.

3. Results and Discussion

The structure of the agarose gel-based ionic power source (AGIPS) is illustrated in Figure 1b. This system comprises five hydrogel layers. High-salinity gels containing concentrated salt solutions are placed at both ends, while a low-salinity gel containing dilute salt solution is positioned at the center to create an ion concentration gradient. At the interfaces between the high- and low-salinity gels, cation- and anion-selective membrane gels are asymmetrically placed. The ion-selective membrane gels are fabricated by incorporating polyelectrolytes into the agarose hydrogels. The polyelectrolyte chains bearing fixed charges are physically entangled within the agarose polymer network, suppressing the transport of co-ions through the electrostatic exclusion. Graphite felt was employed as the current collector and interfaced with the high-salinity gels at both ends. To facilitate electron exchange and sustain charge neutrality at the electrode surfaces, the graphite felt was impregnated with a redox pair of $Fe(CN)_6^{4-}$ and $Fe(CN)_6^{3-}$.

The power generation mechanism of the AGIPS is illustrated in Figure 1c. Upon contact between the gels and exposure to a salinity gradient, directional ion diffusion is driven by Donnan exclusion originating from the fixed charges of the polyelectrolyte membranes, resulting in the formation of an electric potential across the device. Negatively charged polyelectrolyte membranes repel anions, permitting only cations to diffuse into the adjacent low-salinity gel. Conversely, positively charged polyelectrolyte membranes repel cations, selectively allowing anions to migrate. The potential generated across a single selective membrane can be described by the following equation derived from the Goldman–Hodgkin–Katz (GHK) equation (Supporting Information):

$$V_{OC} = \frac{RT}{F} \ln \left(\frac{P_{Na^+} C_{Na^+_{out}} + P_{Cl^-} C_{Cl^-_{in}}}{P_{Na^+} C_{Na^+_{in}} + P_{Cl^-} C_{Cl^-_{out}}} \right) \ , \qquad (2)$$

where R is the gas constant, T is the temperature, F is the Faraday's constant, P_{ion} is the permeability of ions, and C_{ion} is the concentration of ions. This equation highlights that the formation of V_{oc} in AGIPS requires both ion selectivity arising from Donnan exclusion by the polyelectrolyte gel membrane and an ion concentration gradient across the membrane. In the case of an asymmetric arrangement of the cation- and anion-selective membranes, the overall V_{oc} of the AGIPS device is determined by the sum of the potentials generated across the two membranes.

For the efficient charge transfer at the current collector, a redox pair consisting of $Fe(CN)_6^{4-}/Fe(CN)_6^{3-}$ was incorporated. Figure 2a,b compare the V_{oc} and J_{sc} of the AGIPS,

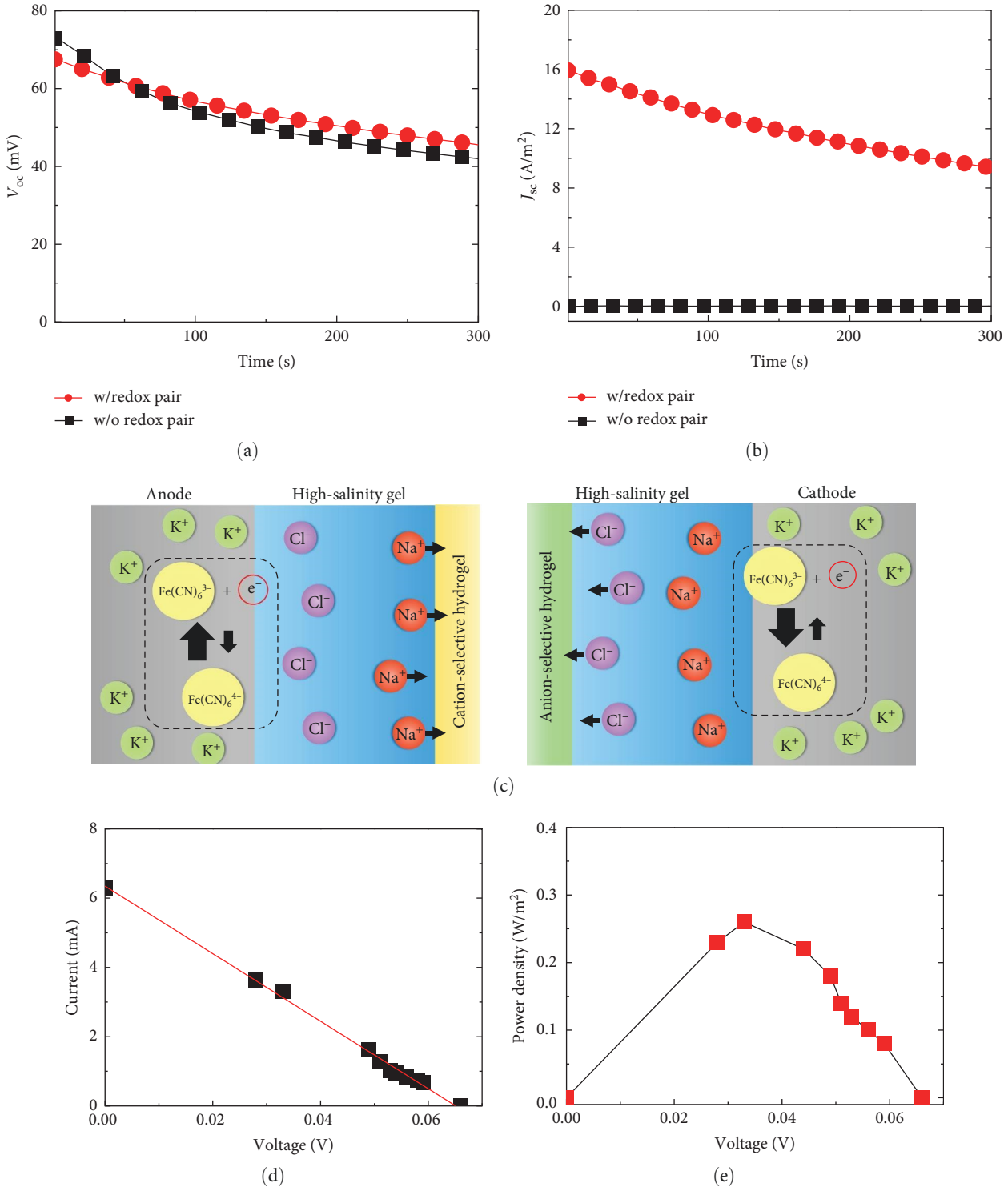

FIGURE 2: Time-dependent (a) V_{oc} and (b) J_{sc} of the AGIPS. (c) Schematic illustrating the role of the redox pair at the electrode–high-salinity gel interfaces. (d) Current and voltage response of the AGIPS and (e) the resulting output power density plot. For the measurement in (d), the AGIPS was connected with various external load resistances in series (Supporting Information). The concentrations of the high- and low-salinity gels were 4 M and 20 mM, respectively.

respectively, in the presence and absence of the redox pair. The results indicate that the V_{oc} did not differ significantly regardless of the inclusion of the redox pair. Therefore, introducing identical redox pairs at both electrodes contributes minimally to V_{oc}, while the V_{oc} is primarily determined by the asymmetric configuration of ion-selective membranes and the ion concentration gradient. Figure 2b, however, shows that the J_{sc} was markedly affected by the presence of the redox pair. AGIPS

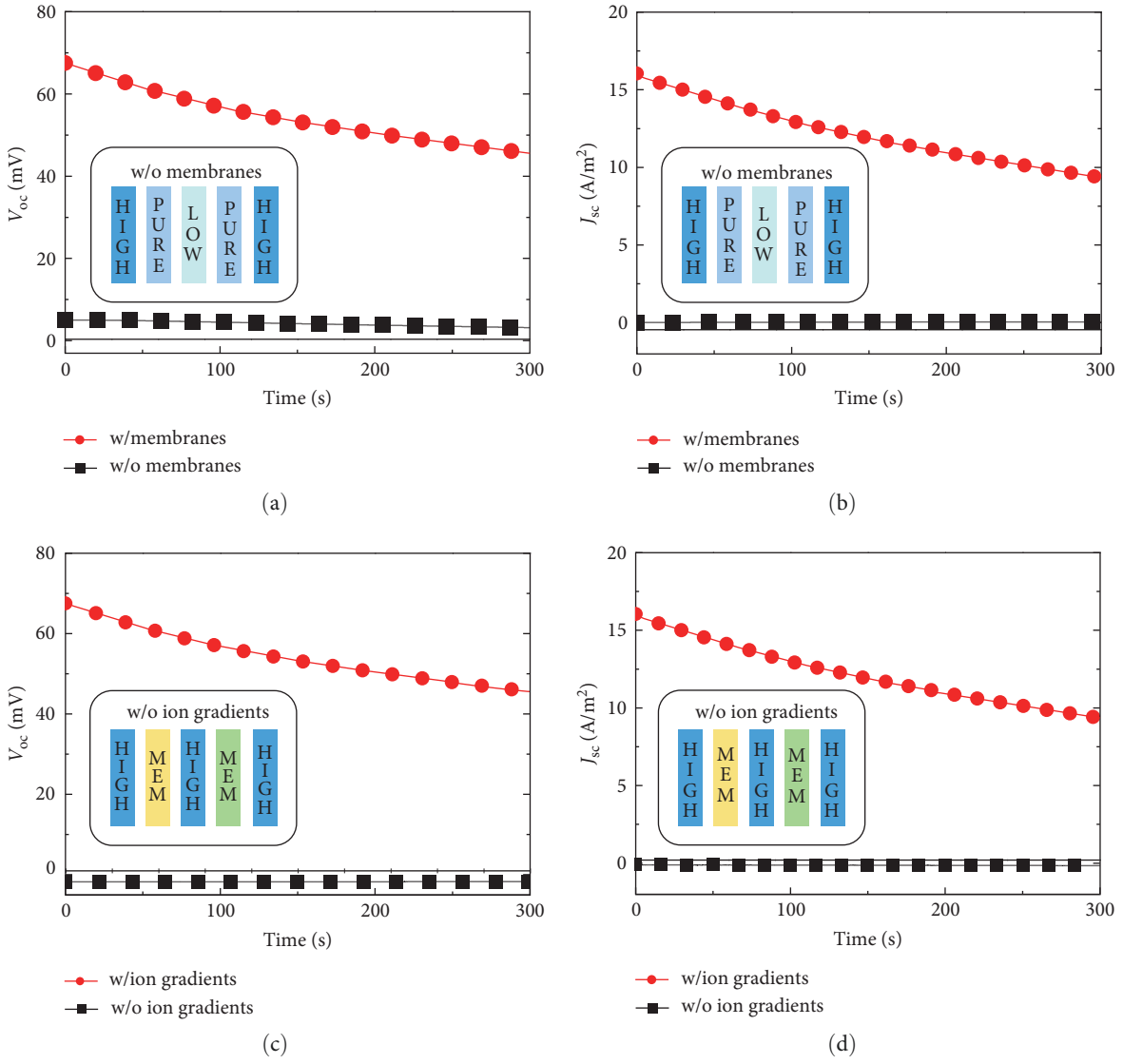

FIGURE 3: (a) V_{oc} and (b) J_{sc} of AGIPS devices with and without ion-selective membranes. (c) V_{oc} and (d) J_{sc} of AGIPS devices with and without ion concentration gradients.

incorporating the redox pair exhibited current densities over 20 times higher than those without it. This significant improvement is due to the ferrocyanide/ferricyanide pair's role in mitigating charge imbalance, as depicted in Figure 2c. Without the redox pair, the unidirectional migration of ions from the high- to low-salinity gel leads to charge imbalance at the electrodes, suppressing continuous electron transfer. Upon introduction of the ferrocyanide/ferricyanide redox pair, reversible redox reactions occur. At the anode, where Na^+ ions are depleted, $Fe(CN)_6^{4-}$ is oxidized to $Fe(CN)_6^{3-}$, releasing electrons. Conversely, at the cathode, where Cl^- ions are depleted, $Fe(CN)_6^{3-}$ is reduced to $Fe(CN)_6^{4-}$, accepting electrons. In this way, the redox pair mitigates the charge imbalance caused by selective ion transport, thereby facilitating electron flow and significantly enhancing output current, as shown in Figure 2b.

To evaluate the power density of the AGIPS device, various external load resistances were connected in series, and the corresponding current–voltage responses were measured (Figure 2d and Supporting Information). Figure 2e shows the calculated power density derived from the current–voltage curve. The device achieved a maximum power density of 0.28 W m^{-2} when the voltage reached approximately half of the open-circuit voltage (V_{oc}/2), which is consistent with the maximum power transfer theorem [4, 6, 7].

According to Equation (1), the primary origin of the voltage and current generation in AGIPS devices arises from the asymmetric arrangement of ion-selective membranes in conjunction with the ionic concentration gradient. Figure 3a,b compare the V_{oc} and J_{sc} of AGIPS devices with ion-selective membranes to those of devices containing non-selective agarose gels without polyelectrolytes. The device lacking ion-selective membranes exhibits negligible V_{oc} and J_{sc}, as the absence of cation- and anion-selective membranes renders the device structurally symmetric. Consequently, no electric potential is established across the device, thereby preventing any net charge migration or current generation. The measured

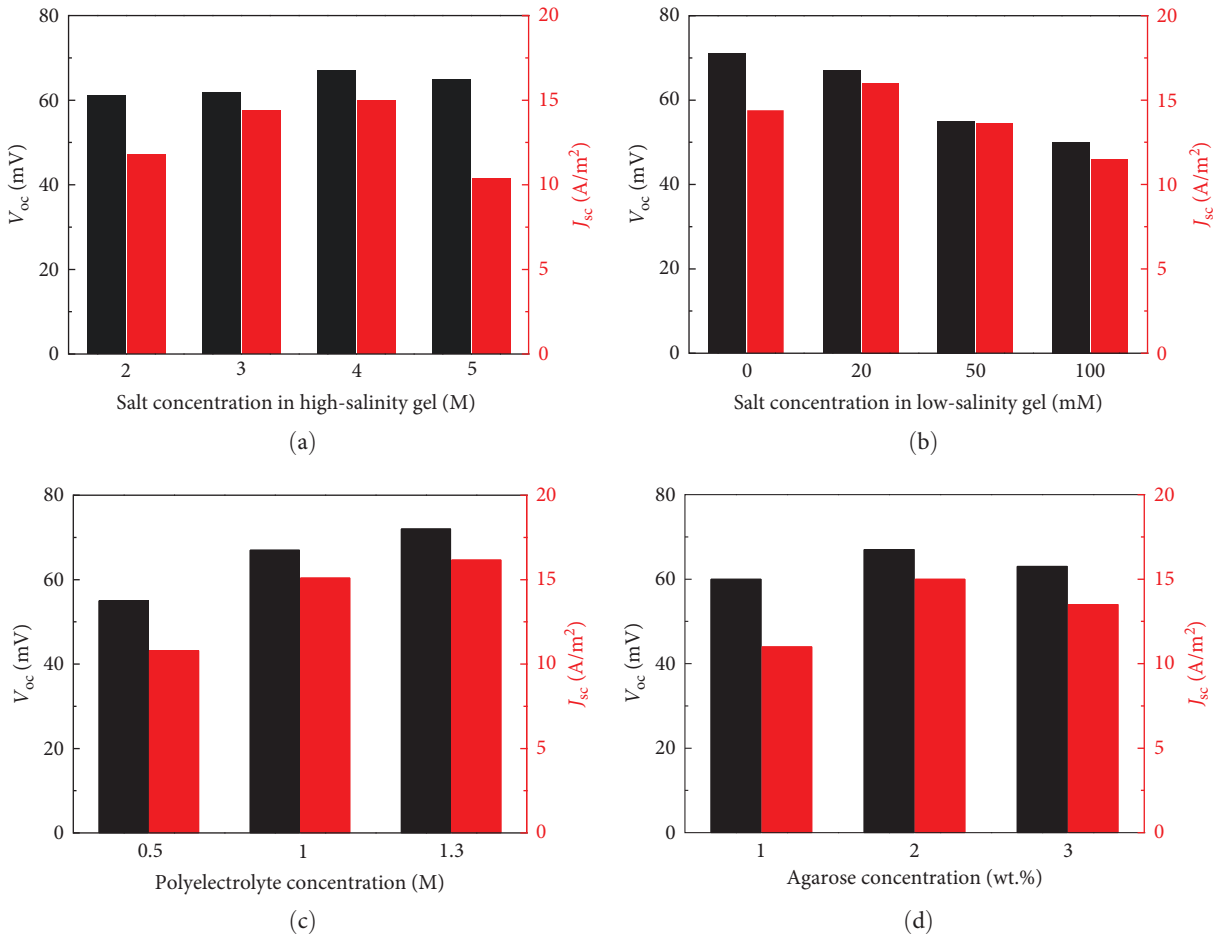

FIGURE 4: V_{oc} and J_{sc} of AGIPS devices as a function of the concentrations of various components incorporated into the system. (a) Salt concentrations in the high-salinity gels, (b) salt concentrations in the low-salinity gels, (c) polyelectrolyte concentrations of the membranes, and (d) agarose contents of the salinity gels.

V_{oc} and J_{sc} of AGIPS devices, in comparison with control devices lacking ion concentration gradients, are presented in Figure 3c,d. To eliminate the gradients, the low-salinity gel in the original AGIPS configuration was replaced with a high-salinity gel, forming a uniform ion concentration across all layers. The control device exhibits negligible V_{oc} and J_{sc}. These results confirm that both the asymmetric ion-selective membrane configuration and the presence of ion concentration gradients are the essential prerequisites for generating electrical potential and current in the system.

Given that the electrochemical output of AGIPS is governed by the ion concentration gradients and the charge selectivity of the polyelectrolyte membranes, modulating the concentrations of ions and polyelectrolytes is expected to significantly impact device performance, and their effects were therefore systematically investigated. Figure 4a shows V_{oc} and J_{sc} values of AGIPS as a function of salt concentrations in the high-salinity gel, while maintaining the low-salinity gel at 20 mM NaCl. Increasing the high-salinity concentration from 2 to 4 M proportionally enhanced both current and voltage, but further increase to 5 M led to a decline in both. This reduction is attributed to incomplete NaCl dissolution at 5 M, resulting in visible precipitation on the hydrogel surface after gelation. Moreover, the mechanical integrity of the gel layers deteriorated, likely due to disruption of hydrogen bond-mediated crosslinking within the agarose network at high ionic strength.

As the ion concentration in the low-salinity gel was varied with the high-salinity gel fixed at 4 M NaCl, the corresponding measurements are illustrated in Figure 4b. Consistent with prior observations, a larger difference in salinity between the two gels enhances the ionic driving force, leading to increased V_{oc} and J_{sc}. As the low-salinity gel concentration increased from 20 to 100 mM, both current and voltage gradually declined. Notably, when the low-salinity gel contained no added salt (0 mM), the current decreased sharply, which can be attributed to markedly reduced ionic conductivity and higher internal resistance.

The influence of the polyelectrolyte concentration in ion-selective membranes on the current and voltage output of AGIPS is demonstrated in Figure 4c. As the polyelectrolyte concentration increased, the V_{oc} and J_{sc} improved, likely due to enhanced ion selectivity. However, excessively high concentrations impeded the formation of robust gel networks during gelation, compromising the mechanical stability of the

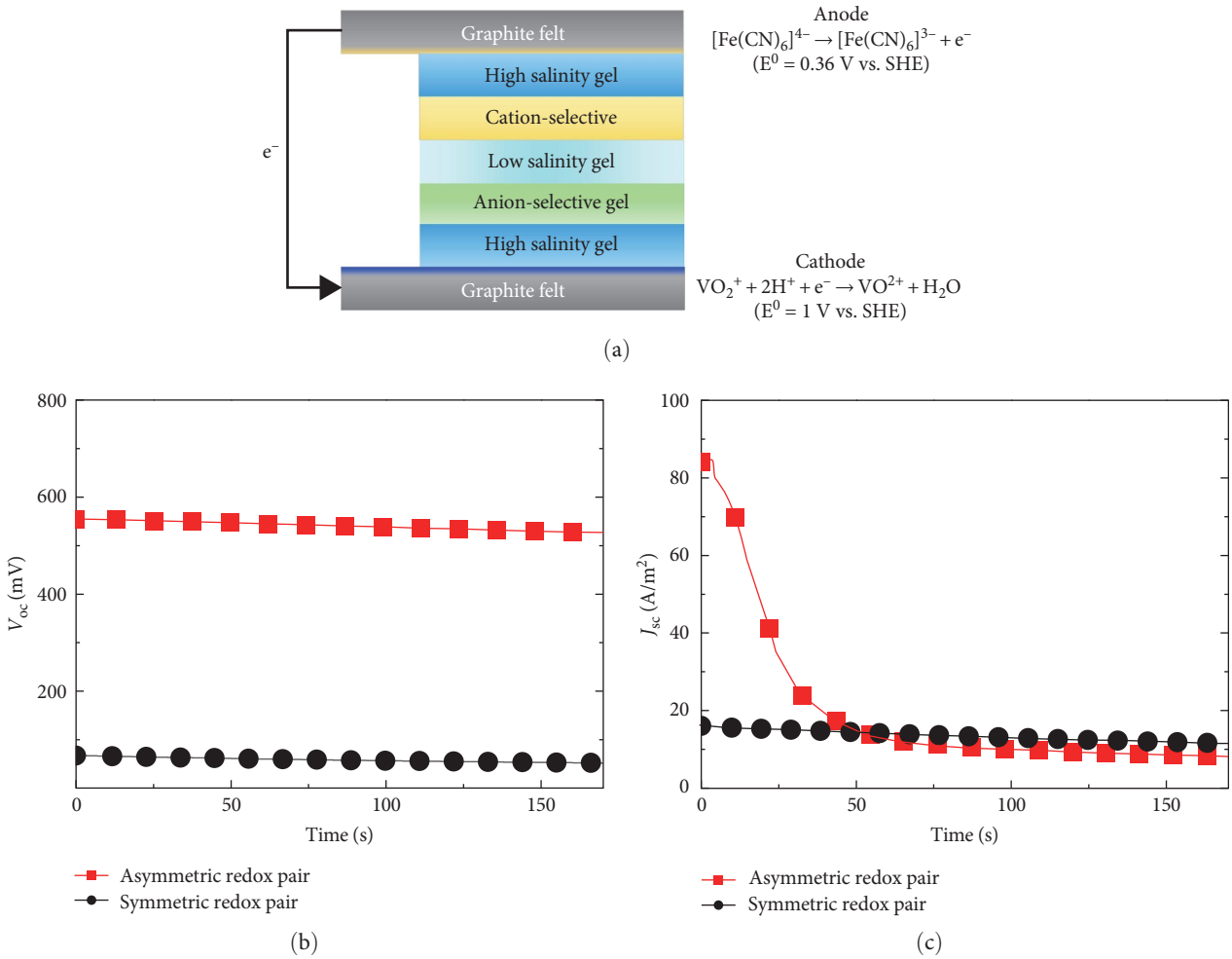

FIGURE 5: (a) Schematic illustration of the AGIPS configuration incorporating asymmetric redox pairs. (b) V_{oc} and (c) J_{sc} of AGIPS devices employing symmetric and asymmetric redox pairs.

hydrogel and the reproducibility of device fabrication. In this study, the concentration of 1 M was selected as the optimal polyelectrolyte concentration to ensure reliable device fabrication.

Agarose content significantly affects the mechanical properties and ionic conductivity of the resulting gel. Generally, increasing the agarose concentration enhances the mechanical strength of the gel, thereby improving the reproducibility of device assembly. However, excessive agarose content leads to the formation of dense polymer networks that impede ion transport in the gel. Figure 4d shows the effect of varying agarose content in the high- and low-salinity gels on the current and voltage output. Both V_{oc} and J_{sc} reached their maximum at an agarose concentration of 2 wt.%. At 3 wt.% agarose, both values decreased relative to those at 2 wt.%, presumably due to decreased ionic conductivity. At 1 wt.% agarose, both were lowest. One possible reason is that the lower agarose content in the salinity gels, compared to the polyelectrolyte membrane gels (3 wt.% agarose), created an osmotic effect that drew water into the membrane gels and reduced the effective polyelectrolyte concentration. Based on these results, 2 wt.% agarose was determined to be the optimal concentration for the AGIPS device.

In our baseline AGIPS configuration, redox pairs were employed symmetrically, contributing primarily to current generation without affecting the potential. However, introducing asymmetric redox pairs with distinct electrode potentials at each side can potentially enhance the overall potential output. To achieve this, we introduced the vanadium oxide redox pair (VO^{2+}/VO_2^{+}) at the cathode, which possesses a more positive electrode potential as shown in Figure 5a. The electrode potential of the vanadium oxide redox pair (1.0 V vs. SHE) is higher than that of the ferrocyanide/ferricyanide pair (0.36 V vs. SHE), thereby enabling an increased potential difference across the electrodes.

A comparison of the voltage and current output of the AGIPS devices with symmetric and asymmetric redox pairs applied at both electrodes is shown in Figure 5b,c. When an asymmetric redox pair was applied, the device produced a V_{oc} exceeding 500 mV, approximately eight times higher than that of the symmetric configuration. Such voltage levels are significantly higher than those reported for a single cell in previously

published studies [4–7]. The elevated V_{oc} was maintained without significant decay over time. This contrasts with the symmetric configuration, where the V_{oc} decreased more significantly over time (Figure 2a). Notably, the ferrocyanide/ferricyanide redox pair carries a negative charge, which can lead to diffusion losses at the cathode through the anion-selective membrane. In contrast, the positively charged vanadium oxide redox pair is likely retained near the cathode, minimizing undesired diffusion through the membrane and thereby contributing to output voltage stability. The initial J_{sc} was also five times higher in the asymmetric redox pair system. However, this elevated current rapidly declined, eventually reaching levels comparable to those in the symmetric case. This transient behavior suggests that the initial current output is primarily governed by charge transfer kinetics driven by the large potential difference, while over time, the mass transport limitations progressively dominate, diminishing the impact of the asymmetric redox pair configuration. To confirm the role of the asymmetric redox pair, we compared the V_{oc} and J_{sc} of AGIPS devices containing the asymmetric redox pairs under conditions with and without ion-selective membranes and with and without ion concentration gradients (Figure S3). These measurements consistently showed that the asymmetric redox configuration significantly increased V_{oc}, whereas J_{sc} was predominantly governed by the presence of the ionic gradient and the membrane selectivity. Overall, these results demonstrate that electrode potential engineering using appropriate redox pairs enables the AGIPS device to generate a more stable and enhanced voltage output while producing elevated initial currents.

The intrinsic challenge in the AGIPS device is that ion diffusion from the high-salinity gel to the low-salinity gel causes the concentration gradient to gradually diminish, eventually leading to the equilibration of ion concentrations and terminating voltage and current generation. To enable extended operation of AGIPS, a flow system that sustains the ionic gradient was introduced, analogous to the operational principle of a RED power plant. Figure 6a illustrates the AGIPS configuration incorporating flow channels. In this setup, a high-concentration source solution flows adjacent to the high-salinity gel layers, while a low-concentration drain solution flows through the middle layer adjacent to the low-salinity gel. A 6 M NaCl aqueous solution and DI water were used as the source and drain solutions, respectively.

Numerical simulations were conducted to predict the temporal evolution of the ion concentration distribution within the gels, depending on the presence or absence of the flow system. Figure 6b presents the simulation results for the AGIPS configuration with integrated flow channels. In the simulations, the flow rates of the source and drain solutions were assumed to be sufficiently high to maintain steady-state boundary concentrations at 6 and 0 M, respectively. After 1000 s, a continuous concentration gradient was established across the gels. As time progressed, the gradient slope slightly decreased; however, a near steady-state distribution was achieved after approximately 3000 s, with minimal further changes in concentration. The simulation results for the standard AGIPS system without the flow system are shown in Figure 6c. As expected, over time, diffusion leads to a gradual decrease in the ion concentration within the high-salinity gel and a corresponding increase in the low-salinity and ion-selective gels. After 6000 s, the ionic concentrations within all gels converged to similar levels, eliminating further potential and current generation.

To assess the extended operational capability enabled by the flow system, an AGIPS device with the configuration shown in Figure 6a was fabricated as shown in Figure S2, and its time-dependent V_{oc} and J_{sc} were monitored. Figure 6d,e show the V_{oc} and J_{sc} retention of AGIPS devices with and without the flow system, respectively. In the absence of the flow system, both V_{oc} and J_{sc} continuously declined, approaching zero within 100 min. In contrast, when the flow system was employed, both values initially declined due to the relaxation of the ion concentration gradient, but subsequently stabilized after 40–50 min, as the gradient was maintained by continuous replenishment from the source and drain flows. These findings confirm that the experimental results closely align with the simulation predictions and validate the long-term operational feasibility of AGIPS devices integrated with the flow system.

4. Conclusion

In this study, we developed the agarose gel-based power source inspired by the electrochemical energy generation mechanism of electric fish. By integrating high- and low-salinity hydrogels with asymmetric ion-selective polyelectrolyte membranes, the device generated V_{oc} and J_{sc} driven by ion concentration gradients and Donnan exclusion effects. Systematic optimization of the material compositions revealed that a high-salinity gel concentration of 4 M NaCl and a low-salinity gel concentration of 20 mM NaCl achieved the highest performance, while an agarose content of 2 wt.% provided the best balance between ionic conductivity and mechanical stability. Importantly, incorporating asymmetric redox pairs, specifically ferrocyanide/ferricyanide at the anode and vanadium oxide at the cathode, significantly enhanced the voltage and current output while mitigating charge imbalance during operation. To address the intrinsic performance decay caused by ionic gradient depletion over time, the flow system was implemented to continuously replenish the high- and low-salinity conditions. Numerical simulations and experimental validation demonstrated that the flow-assisted configuration effectively maintained the ionic gradient, enabling sustained voltage and current output over extended durations. In particular, the current and voltage retention measurements showed strong agreement with simulation predictions, confirming the long-term operational feasibility of the system.

Overall, the proposed AGIPS device demonstrates a safe, robust, scalable, and environmentally benign platform for generating electricity. The combination of material optimization, electrode potential engineering via asymmetric redox pairs, and maintenance of ion gradients through flow channels offers an effective strategy to enhance both the performance and durability of the hydrogel-based power systems. This work provides valuable insights into the design of next-generation bio-inspired energy harvesters and paves the way for future

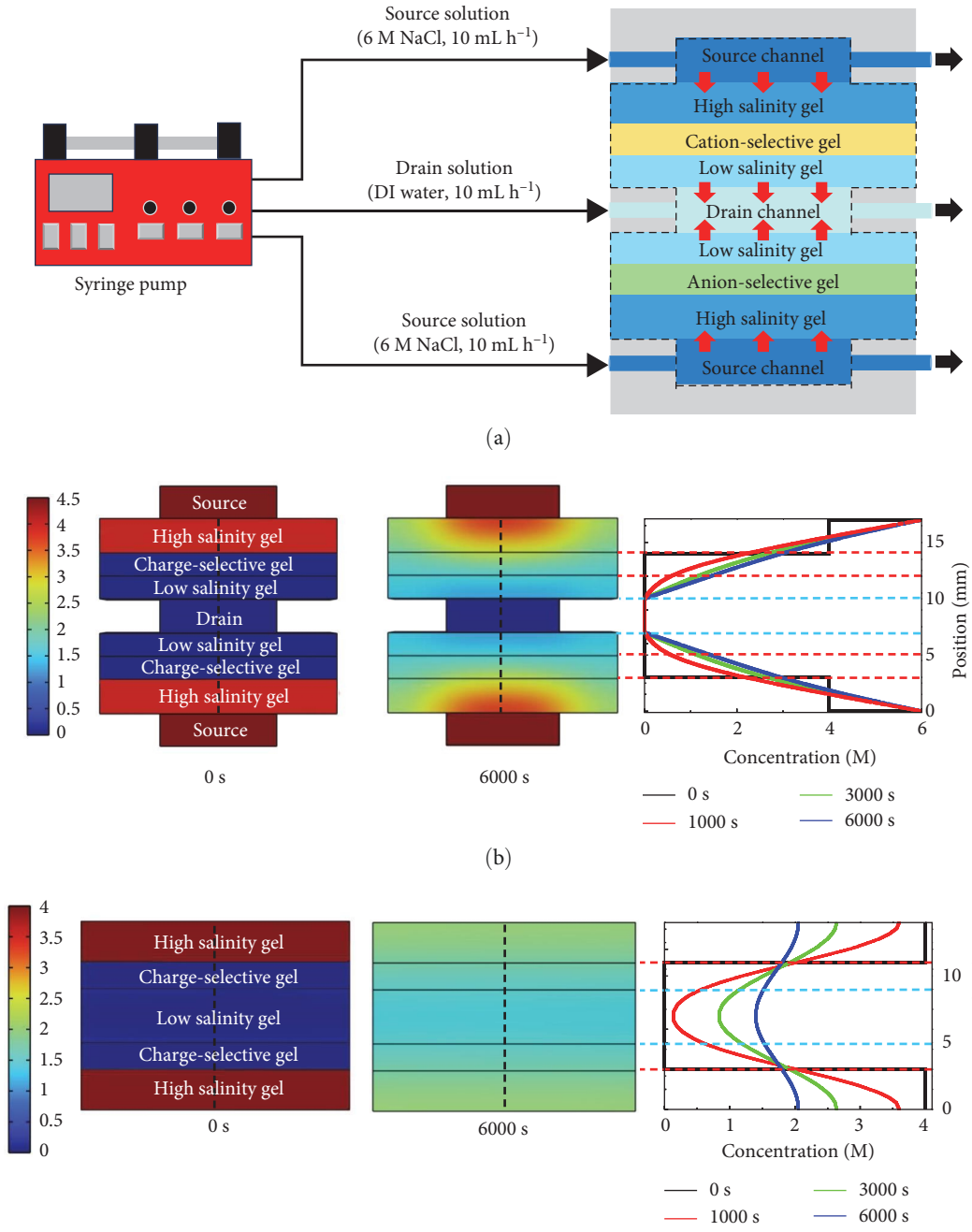

Figure 6: Continued.

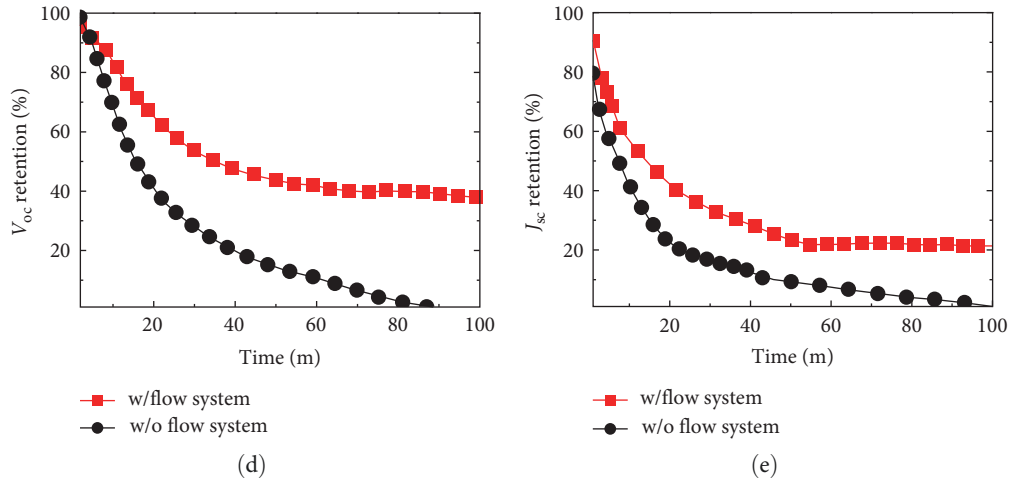

FIGURE 6: (a) Schematic illustration of the AGIPS device integrated with a flow system. The source and drain channels deliver high- and low-concentration salt solutions adjacent to the high-salinity and low-salinity gels, respectively. (b, c) Simulation results for the AGIPS devices (b) with and (c) without the flow system, showing the ion concentration distributions (color maps) and the time-dependent concentration profiles along the dashed lines indicated in the color maps. The simulation dimensions were identical to those of the actual devices. (d) V_{oc} retention and (e) J_{sc} retention of AGIPS devices with and without the flow system.

applications in sustainable power generation for soft robotics [43], on-body electronics [44], and wearable sensor systems [45].

Data Availability Statement

The data that support the findings of this study are available from the corresponding author upon reasonable request.

Conflicts of Interest

The authors declare no conflicts of interest.

Author Contributions

Sung-Hyun Kim and Yang-Woo Lee contributed equally to this work.

Funding

This work was supported by the International Collaborative Research and Development Program (Grant P0028061) and Joint R&D Project of the Global Industrial Technology Cooperation Center (Grant P0028921) funded by the Ministry of Trade, Industry and Energy (MOTIE, Republic of Korea). This work also has been supported by the National Research Foundation of Korea (NRF) grant funded by the Ministry of Science and ICT of Korea government (Grant RS-2024-00451691).

Supporting Information

Additional supporting information can be found online in the Supporting Information section. (*Supporting Information*)
The Supporting Information provides detailed descriptions of the derivation procedure of output voltage in AGIPS derived from GHK equation and the measurement of current-voltage responses and power density of AGIPS.

References

[1] J. R. Gallant, L. L. Traeger, J. D. Volkening, et al., "Genomic Basis for the Convergent Evolution of Electric Organs," *Science* 344, no. 6191 (2014): 1522–1525.
[2] R. D. Keynes and H. Martins-Ferreira, "Membrane Potentials in the Electroplates of the Electric Eel," *The Journal of Physiology* 119, no. 2-3 (1953): 315–351.
[3] A. L. Gotter, M. A. Kaetzel, and J. R. Dedman, "*Electrophorus electricus* as a Model System for the Study of Membrane Excitability," *Comparative Biochemistry and Physiology Part A: Molecular & Integrative Physiology* 119, no. 1 (1998): 225–241.
[4] T. B. H. Schroeder, A. Guha, A. Lamoureux, et al., "An Electric-Eel-Inspired Soft Power Source From Stacked Hydrogels," *Nature* 552, no. 7684 (2017): 214–218.
[5] P. He, J. He, Z. Huo, and D. Li, "Microfluidics-Based Fabrication of Flexible Ionic Hydrogel Batteries Inspired by Electric Eels," *Energy Storage Materials* 49 (2022): 348–359.
[6] Y. Zhang, J. Riexinger, X. Yang, et al., "A Microscale Soft Ionic Power Source Modulates Neuronal Network Activity," *Nature* 620, no. 7976 (2023): 1001–1006.
[7] A. Guha, T. J. Kalkus, T. B. H. Schroeder, et al., "Powering Electronic Devices From Salt Gradients in AA-Battery-Sized Stacks of Hydrogel-Infused Paper," *Advanced Materials* 33, no. 31 (2021): 2101757.
[8] G. G. Bütün, A. Yürüm, S. A. Gürsel, and A. Koşar, "Polymer Based Electricity Generation Inspired by Eel Electrocytes," *International Journal of Energy Research* 46, no. 15 (2022): 22653–22663.
[9] D. Jiao, Q. L. Zhu, C. Y. Li, Q. Zheng, and Z. L. Wu, "Programmable Morphing Hydrogels for Soft Actuators and Robots: From Structure Designs to Active Functions," *Accounts of Chemical Research* 55, no. 11 (2022): 1533–1545.
[10] X. P. Hao, Z. Xu, C. Y. Li, W. Hong, Q. Zheng, and Z. L. Wu, "Kirigami-Design-Enabled Hydrogel Multimorphs With Application as a Multistate Switch," *Advanced Materials* 32, no. 22 (2020): 2000781.
[11] K. Varaprasad, C. Karthikeyan, M. M. Yallapu, and R. Sadiku, "The Significance of Biomacromolecule Alginate for the 3D

Printing of Hydrogels for Biomedical Applications," *International Journal of Biological Macromolecules* 212 (2022): 561–578.

[12] K. Go, D.-M. Kim, and K. J. Lee, "3D Printable Hydrogel Filament With Functionalizable Moiety for in-Situ Flow-Based Sensor," *Macromolecular Research* 32, no. 5 (2024): 467–473.

[13] K. Park, Y. Jeon, J. Bae, S. Kim, and D.-S. Shin, "One-Pot Preparation of Alpha-Chymotrypsin Degradable Hydrogel Micropatterns for Controlled Drug Release," *Korean Journal of Chemical Engineering* 41, no. 9 (2024): 2651–2659.

[14] D. Moon, K. H. Song, and J. Doh, "Jammed Microgels Fabricated via Various Methods for Biological Studies," *Korean Journal of Chemical Engineering* 40, no. 2 (2023): 267–275.

[15] V. Normand, D. L. Lootens, E. Amici, K. P. Plucknett, and P. Aymard, "New Insight Into Agarose Gel Mechanical Properties," *Biomacromolecules* 1, no. 4 (2000): 730–738.

[16] Y. Wang, S. Ding, M. Gong, S. Xu, W. Xu, and C. Zhang, "Diffusion Characteristics of Agarose Hydrogel Used in Diffusive Gradients in Thin Films for Measurements of Cations and Anions," *Analytica Chimica Acta* 945 (2016): 47–56.

[17] C. T. Buckley, S. D. Thorpe, F. J. O'Brien, A. J. Robinson, and D. J. Kelly, "The Effect of Concentration, Thermal History and Cell Seeding Density on the Initial Mechanical Properties of Agarose Hydrogels," *Journal of the Mechanical Behavior of Biomedical Materials* 2, no. 5 (2009): 512–521.

[18] C. Aaij and P. Borst, "The Gel Electrophoresis of DNA," *Biochimica et Biophysica Acta (BBA) - Nucleic Acids and Protein Synthesis* 269, no. 2 (1972): 192–200.

[19] P. Y. Lee, J. Costumbrado, C.-Y. Hsu, and Y. H. Kim, "Agarose Gel Electrophoresis for the Separation of DNA Fragments," *Journal of Visualized Experiments* 62, no. 62 (2012).

[20] G. R. López-Marcial, A. Y. Zeng, C. Osuna, J. Dennis, J. M. García, and G. D. O'Connell, "Agarose-Based Hydrogels as Suitable Bioprinting Materials for Tissue Engineering," *ACS Biomaterials Science & Engineering* 4, no. 10 (2018): 3610–3616.

[21] T. Su, M. Zhang, Q. Zeng, et al., "Mussel-Inspired Agarose Hydrogel Scaffolds for Skin Tissue Engineering," *Bioactive Materials* 6, no. 3 (2021): 579–588.

[22] S. Yu and C. Cha, "Bioadhesives Based on Multifunctional Biopolymers for Biomedical Applications," *Macromolecular Research* 31, no. 5 (2023): 427–441.

[23] Y. Dong, S. Li, X. Li, and X. Wang, "Smart MXene/Agarose Hydrogel With Photothermal Property for Controlled Drug Release," *International Journal of Biological Macromolecules* 190 (2021): 693–699.

[24] S. Xiang, C. Guilbaud-Chéreau, P. Hoschtettler, L. Stefan, A. Bianco, and C. Ménard-Moyon, "Preparation and Optimization of Agarose or Polyacrylamide/Amino Acid-Based Double Network Hydrogels for Photocontrolled Drug Release," *International Journal of Biological Macromolecules* 255 (2024): 127919.

[25] C. Zhu, Y. Teng, G. Xie, et al., "Bioinspired Hydrogel-Based Nanofluidic Ionic Diodes: Nano-Confined Network Tuning and Ion Transport Regulation," *Chemical Communications* 56, no. 58 (2020): 8123–8126.

[26] J. Zhao, M. Marczynski, M. Henkel, and O. Lieleg, "Agarose-Based Hydrogels With Tunable, Charge-Selective Permeability Properties," *Journal of Applied Polymer Science* 140, no. 34 (2023).

[27] N. Gogoi, M. Barooah, G. Majumdar, and D. Chowdhury, "Carbon Dots Rooted Agarose Hydrogel Hybrid Platform for Optical Detection and Separation of Heavy Metal Ions," *ACS Applied Materials & Interfaces* 7, no. 5 (2015): 3058–3067.

[28] N. X. D. Mai, J. Bae, I. T. Kim, et al., "A Recyclable, Recoverable, and Reformable Hydrogel-Based Smart Photocatalyst," *Environmental Science: Nano* 4, no. 4 (2017): 955–966.

[29] S. Li, H. Lu, G. Zhu, et al., "A Recyclable and Stable BiOI/Agarose Hybrid Gel Photocatalyst for Photodegradation of Rhodamine B," *Journal of Materials Science: Materials in Electronics* 29, no. 19 (2018): 16454–16459.

[30] H.-J. Koo, S. T. Chang, J. M. Slocik, R. R. Naik, and O. D. Velev, "Aqueous Soft Matter Based Photovoltaic Devices," *Journal of Materials Chemistry* 21, no. 1 (2011): 72–79.

[31] M. J. Lee, D. R. Shrotriya, and R. M. Espinosa-Marzal, "Responsiveness of Charged Double Network Hydrogels to Ionic Environment," *Advanced Functional Materials* 34, no. 37 (2024): 2402279.

[32] Y. H. Fang, C. Liang, V. Liljestrom, Z. Lv, O. Ikkala, and H. Zhang, "Toughening Hydrogels with Fibrillar Connected Double Networks," *Advanced Materials* 36, no. 27 (2024): 2402282.

[33] T. Yan, Y. Zou, X. Zhang, D. Li, X. Guo, and D. Yang, "Hydrogen Bond Interpenetrated Agarose/PVA Network: A Highly Ionic Conductive and Flame-Retardant Gel Polymer Electrolyte," *ACS Applied Materials & Interfaces* 13, no. 8 (2021): 9856–9864.

[34] J. Park, N. Jeon, S. Lee, G. Choe, E. Lee, and J. Y. Lee, "Conductive Hydrogel Constructs With Three-Dimensionally Connected Graphene Networks for Biomedical Applications," *Chemical Engineering Journal* 446 (2022): 137344.

[35] D. A. Vermaas, M. Saakes, and K. Nijmeijer, "Doubled Power Density From Salinity Gradients at Reduced Intermembrane Distance," *Environmental Science & Technology* 45, no. 16 (2011): 7089–7095.

[36] B. E. Logan and M. Elimelech, "Membrane-Based Processes for Sustainable Power Generation Using Water," *Nature* 488, no. 7411 (2012): 313–319.

[37] D. A. Vermaas, J. Veerman, N. Y. Yip, M. Elimelech, M. Saakes, and K. Nijmeijer, "High Efficiency in Energy Generation From Salinity Gradients With Reverse Electrodialysis," *ACS Sustainable Chemistry & Engineering* 1, no. 10 (2013): 1295–1302.

[38] M. Tedesco, C. Scalici, D. Vaccari, A. Cipollina, A. Tamburini, and G. Micale, "Performance of the First Reverse Electrodialysis Pilot Plant for Power Production From Saline Waters and Concentrated Brines," *Journal of Membrane Science* 500 (2016): 33–45.

[39] Y. Su, N. Chan, H. Ren, et al., "Application of Modified Graphite Felt as Electrode Material: A Review," *Carbon Letters* 33, no. 1 (2023): 1–16.

[40] M. Jing, Z. Wei, W. Su, et al., "Improved Electrochemical Performance for Vanadium Flow Battery by Optimizing the Concentration of the Electrolyte," *Journal of Power Sources* 324 (2016): 215–223.

[41] D.-S. Yang, J. Y. Lee, S.-W. Jo, S. J. Yoon, T.-H. Kim, and Y. T. Hong, "Electrocatalytic Activity of Nitrogen-Doped CNT Graphite Felt Hybrid for All-Vanadium Redox Flow Batteries," *International Journal of Hydrogen Energy* 43, no. 3 (2018): 1516–1522.

[42] H.-J. Koo and O. D. Velev, "Design and Characterization of Hydrogel-Based Microfluidic Devices With Biomimetic Solute Transport Networks," *Biomicrofluidics* 11, no. 2 (2017): 024104.
[43] M. Kumar, M. K. Singh, G. Arora, et al., "A Comprehensive Review on Next-Gen Electrospun Nanofibers for Multidirectional Applications From Energy Storage to Precise Medicine," *Macromolecular Research* 37, no. 24 (2025).
[44] R. S. Chen, M. Gao, D. Chu, et al., "Self-Powered Hydrogel Wearable Bioelectronics, Soft Implantable Bioelectronics for the Management of Neurological Disorders and Cardiovascular Diseases," *Korean Journal of Chemical Engineering* 42, no. 9 (2025): 2037–2068.
[45] Y. J. Yang, S. G. Lee, T. Kim, et al., "Wearable Devices for Biofluid Monitoring in a Body: From Lab to Commercialization, Integrated Intelligent Sensing System With WO3/CNTs Sensor for on-Site Gas Detection," *Korean Journal of Chemical Engineering* 42 (2025): 2011–2036.